Hindawi Publishing Corporation
Advances in Materials Science and Engineering
Volume 2015, Article ID 583106, 10 pages
http://dx.doi.org/10.1155/2015/583106

Research Article

Effects of Nano-TiO_2 on the Toughness and Durability of Cement-Based Material

Baoguo Ma, Hainan Li, Junpeng Mei, Xiangguo Li, and Fangjie Chen

State Key Laboratory of Silicate Materials for Architectures, Wuhan University of Technology, Wuhan 430070, China

Correspondence should be addressed to Hainan Li; lihainan2012@126.com

Received 26 March 2015; Accepted 29 June 2015

Academic Editor: João M. P. Q. Delgado

The effects of nano-TiO_2 (NT) on microstructures and mechanical properties of cement mortars were studied by scanning electron microscopy (SEM), X-ray diffraction (XRD), and mercury intrusion porosimetry (MIP). Results show that 3% NT can remarkably increase the tensile/flexural strengths (i.e., the toughness is improved) and promote the precipitation of AFt crystal. The flexural and tensile strengths have significant positive correlation to the formation amount of AFt. The pores of mortars can be significantly refined and shift to harmless pores by controlling the growth of CH crystal and increasing the hydration reaction rate. The durability of cement-based materials is discussed by testing their water absorption and water-vapour permeability. Results show that the addition of 3% NT can decrease the water absorption ratio by 40–65%, water absorption coefficients by more than 40%, and water-vapour permeability coefficients by 43.9%, indicating that 3% NT can effectively improve the compactness and durability of cement-based materials.

1. Introduction

Nano-TiO_2 is widely used as a white paint in cosmetics, food, and other fields due to its low cost, safety, and chemical stability [1]. In the last two decades, the research on nanoparticle modification technology of traditional cement-based materials has attracted much attention [2]. The incorporation of nano-TiO_2 into cementitious materials has recently started to be investigated from different points of view. At first it was used in preparation of white cement to utilize the white color. And later it is perhaps the most well-known photocatalytic semiconductor because it possesses a strong oxidizing capability, so nano-TiO_2 was gradually used in interior furnishing materials and exterior construction materials, such as wallpapers, cement mortars, and dry-mixed concrete paving block [3–5]. Yu et al. [6] have proposed that the organic particles and air pollution, for example, NO_x, can be decomposed by the function of nano-TiO_2, so if the surface of concrete is covered by a layer of nano-TiO_2, the concrete can be functionalized and the city will become cleaner. Such type of concrete has been used on some pavement [7]. The photocatalysis mechanism of nano-TiO_2 has been systematically studied [8–10] and provided a solid theoretical foundation for its application in building materials. On account of strong binding property of cement-based materials, nano-TiO_2 can be conveniently applied in these materials without any further processing. In addition, the porous structures of hardened mortars/concretes are also suitable for the adsorption of nano-TiO_2 particles. Cementitious materials mixed with nano-TiO_2 have the functions of air purification [11], self-cleaning [12], and disinfection [13], which are the reasons for the wide application in the exterior surface of buildings including hospitals, restaurants, and airports.

Although the self-cleaning and disinfection functions of nano-TiO_2 in cementitious materials have been extensively discussed [14], few research has been conducted to examine the effects of nano-TiO_2 on the inherent performance of hardened mortars/concretes, and the present research mainly focused on the effects of nano-TiO_2 on the hydration process of cement. Lee and Kurtis pointed out that nano-TiO_2 is chemically inert in the process of cement hydration, but it can provide crystal nucleuses to promote the cement hydration, leading to the increase of compressive strength of mortars [15]. But so far it remains controversial whether nano-TiO_2 can improve the genetic defects of cement-based materials, including high brittleness and internal cracks, which lead to a decline in performance and service life of building materials.

So the methods to improve toughness of cement composites have become a topic of general interest in recent years.

Currently, the main methods of reducing high brittleness and cracks of cement-based materials are by addition of reinforcing materials such as steel fibers [16], carbon fibers [17], polymer fibers [18–20], and mineral fibers [21, 22]. The purpose is to improve the behavior of cracks-resisting and increase the overall strengths of cement-based materials by the high strength and high toughness of reinforcing materials. However, the addition of reinforcing materials does not change the microstructure of hydration products, and the problems of high brittleness and internal cracks still exist.

In this paper, the effects of nano-TiO_2 on the toughness of hardened mortars were studied by comparing the flexural and tensile strengths of cement-based materials with and without nano-TiO_2, and the mechanism was analyzed by scanning electron microscope (SEM), X-ray diffraction (XRD), and mercury intrusion porosimetry (MIP). In addition, the durability of cement-based materials was assessed by testing their water absorption and water-vapour permeability.

2. Experimental Program

2.1. Materials. A sample of P·O42.5 cement was obtained from Huaxin cement Co. Ltd. and its chemical composition is listed in Table 1. The medium coarse river sand was produced by Hubei Xishui Hualiangting quarry and its fineness modulus is 2.8. The limestone, which is continuously graded, was used as coarse aggregate, where particle distribution is 5–20 mm. The 2651F polycarboxylate superplasticizer (SP) admixture was provided by BSAF (China) Co. Ltd. The fumed nanotitanium dioxide (NT) provided by Germany presents a specific surface area of 50 m^2/g and its TEM image is shown in Figure 1.

AFt was produced by precipitation reaction of $Al_2(SO_4)_3{\cdot}18H_2O$ (chemically pure) and CaO (chemically pure) by a molar ratio of 1 : 6. Firstly, some distilled water was added to CaO to produce supersaturated solution. Then, the prepared CaO solution was slowly added to $Al_2(SO_4)_3{\cdot}18H_2O$. After being stirred for 8 h by the magnetic stirrer, the mixed solution was sealed for 7 days for complete reaction and precipitation. Finally, the resultant powders were washed with absolute ethanol and filtered by a vacuum pump until a constant weight is obtained. Figure 2 shows the XRD patterns of synthetic AFt, where purity calculated by software of MDI Jade 5.0 is 98.96%, and others are tiny amounts of dihydrate gypsum.

2.2. Specimen Preparation. Mix proportions of test specimens are shown in Table 2. The specimens used to test flexural strength and tensile strength of mortars were molded by 40 mm × 40 mm × 160 mm and 100 mm × 100 mm × 400 mm triple moulds, respectively, and concrete specimens were molded by 100 mm × 100 mm × 100 mm triple moulds. After 24 h they were demoulded and the specimens were stored in a climatic chamber (20°C, 95% relative humidity) until they reached the test age.

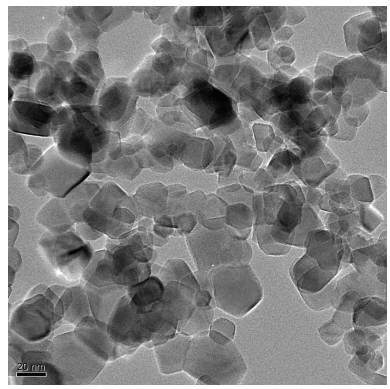

Figure 1: TEM image of nano-TiO_2.

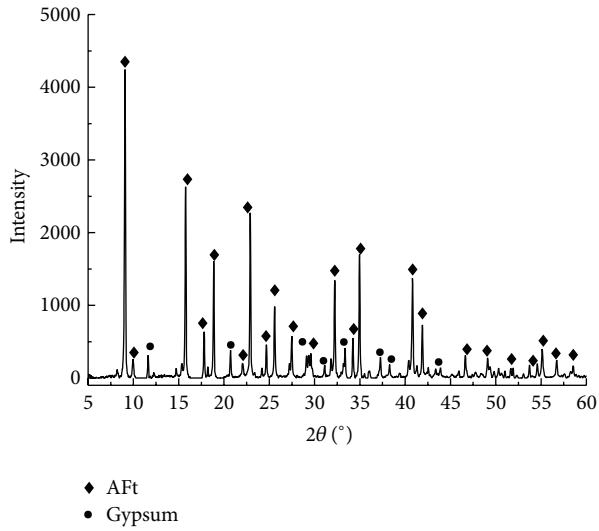

Figure 2: XRD pattern of synthetic AFt.

After curing for 27 days, the specimens of M0 and M3 and concretes were cut into small pieces of 40 mm × 40 mm × 10 mm and 100 mm × 100 mm × 10 mm, respectively, by cold saw-cutting-off machine, making each piece used to test water absorption have two parallel planes. The mortars for water-vapour permeability test were molded in plastic beakers of 500 mL for 1 day. After curing in standard curing box for 27 days, the specimens were cut into small cylinders about 10 mm in thickness. Water-vapour permeabilities of sealed and unsealed mortars were experimentally studied, and specimen seal was implemented with scotch tape. Also, sealed samples were cured in the same environment for the same temperature and humidity as the samples unsealed. Before starting the water-vapour permeability test, scotch tape was removed from the surface of sample, and then ultrasonic cleaner was used for further removal of the attachments.

2.3. Performance Test. The method of water absorption test has been reported in previous work [23]. After being dried at 60°C for 48 h in the oven, the samples of mortars and

Table 1: Chemical composition of cement (wt%).

Composition (wt%)	SiO_2	CaO	Al_2O_3	Fe_2O_3	MgO	SO_3	K_2O	Na_2O	TiO_2	Loss
P·O42.5	21.50	65.20	4.14	2.40	2.57	2.89	0.84	0.67	0.32	2.67

Table 2: Mix proportions of test specimens.

Code number	Water-to-cement ratio	Mix proportion kg/m^3					
		Cement	NT	Sand	Stone	Water	SP
M0	0.58	450.0	0.0	1350	—	261	9.0
M1	0.58	445.5	4.5	1350	—	261	9.0
M2	0.58	441.0	9.0	1350	—	261	9.0
M3	0.58	436.5	13.5	1350	—	261	9.0
M4	0.58	432.0	18.0	1350	—	261	9.0
M5	0.58	427.5	22.5	1350	—	261	9.0
C1	0.45	420.0	0.0	634	1177	189	8.4
C2	0.45	407.4	12.6	634	1177	189	8.4
C3	0.58	300.0	0.0	672	1248	174	—
C4	0.58	291.0	9.0	672	1248	174	—

concretes cut into pieces were weighed and then placed in a basin. The specimens soaked in water for 10, 20, 40, and 90 min were also weighed, respectively, when the saturated surface was dry, and then the increasing value of masses of specimens with different dipped time was calculated. Water absorption ratio, namely, water absorption mass per unit area, can be obtained by dividing the increasing mass value by the surface area of specimens. The water absorption coefficient can be characterized by the slope of curve of water absorption over square root of soaking time (s) at early stage.

Water-vapour permeabilities of mortars were tested by the wet cup method [24]. The cup was separated into inside part and outside part by cylindrical mortar samples. The relative humidity condition outside was controlled to 60% by saturated solutions of KBr and that inside was adjusted to about 100% by tap water. Because the water vapour diffused from wet cup to saturated salt solutions, the cup was losing weight. Water-vapor permeability can be reflected by the plot of the mass of wet cup as a function of time. The samples (10 mm thick and 80 mm in diameter) and plastic cups should be sealed by sealants to make the inside condition of wet cup strictly separate from the outside condition of saturated KBr solution.

Crystal phases were characterized by X-ray diffraction analysis (XRD, Bruker, D8 Advance, Cu K_α) under operating voltage of 40 kV, working current of 100 mA, graphite bend crystal monochromator as optical filter, and scanning mode with 0.02° per step and stopping 4 s before the next.

AFt content in each age was quantified with external standard method. The samples were produced from unhydrated Portland cements, which were mixed with the 5, 10, 15, and 20 wt% AFt and then ground in agate mortars for 10 min, respectively. After preparation of the samples, XRD patterns of AFt from 8.5° to 9.5° were measured using the above scanning mode. Each test was repeated three times and took the mean to eradicate any discrepancies. The external standard curve of integrated intensity as a function of the content of synthetic AFt is shown in Figure 3. With the method of fitting, the linear fitting equation is the most effective, and the relationship between (y) integral intensities of AFt characteristic peak and (x) the content of synthetic AFt can be represented by equation as

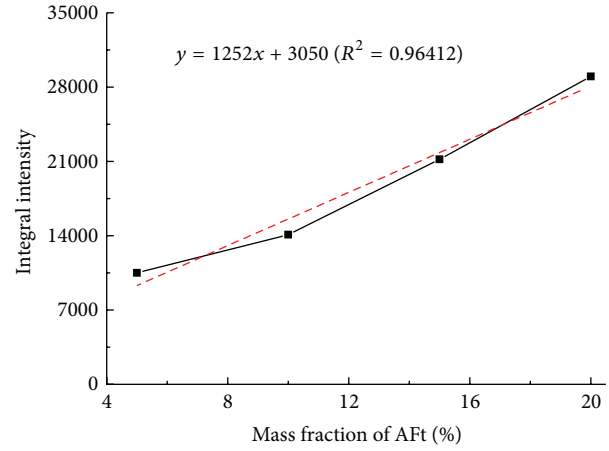

Figure 3: External standard curves of synthetic AFt.

$$y = 1252x + 3050 \quad \left(R^2 = 0.96412\right). \tag{1}$$

The integral intensity of AFt in each age can be calculated by importing diffraction data to MDI Jade 5.0 software, and then the content of AFt forming in the hydration process can be obtained by (1).

The surface morphologies were confirmed by a scanning electron microscope (SEM, Jeol, JSM-6360LV). The pore distributions of hardened mortars were obtained by mercury intrusion porosimetry (MIP, Quantachrome Ltd., PM-60-GT).

Table 3: Tensile and flexural strengths of mortars with different dosages of NT.

Sample designation/nano-TiO_2 dosage (%)	Tensile strength (MPa)/increase rate (%)			Flexural strength (MPa)/increase rate (%)		
	3 days	28 days	90 days	3 days	28 days	90 days
M0/0	1.05 ± 0.02/0	3.36 ± 0.12/0	5.60 ± 0.21/0	2.82 ± 0.11/0	4.42 ± 0.17/0	6.28 ± 0.29/0
M1/1	1.35 ± 0.03/28.6	4.95 ± 0.23/47.3	7.01 ± 0.32/25.2	4.28 ± 0.18/51.8	6.71 ± 0.29/51.8	8.19 ± 0.34/30.4
M2/2	1.39 ± 0.04/32.3	5.35 ± 0.22/59.2	7.23 ± 0.29/29.1	4.34 ± 0.21/53.9	6.88 ± 0.32/55.7	8.57 ± 0.31/36.5
M3/3	1.59 ± 0.06/51.4	5.65 ± 0.19/68.2	7.65 ± 0.35/36.6	4.56 ± 0.12/61.7	7.12 ± 0.27/61.9	9.05 ± 0.25/44.1
M4/4	1.31 ± 0.02/24.8	4.66 ± 0.15/38.7	6.66 ± 0.14/18.9	3.62 ± 0.08/28.4	5.77 ± 0.12/30.5	7.56 ± 0.22/20.4
M5/5	1.30 ± 0.02/23.7	4.63 ± 0.21/37.8	6.61 ± 0.22/18.0	3.61 ± 0.05/28.0	5.76 ± 0.15/30.3	7.43 ± 0.19/18.3

3. Results and Discussion

3.1. Impact of NT on Mechanical Properties and Microstructures of Mortars. The tensile and flexural strengths of mortars with different dosage of NT are listed in Table 3. Results show that the tensile and flexural strengths increase with increasing NT content up to 3%. Further increasing the NT content, the tensile and flexural strengths decrease slightly instead. The tensile and flexural strengths of M3 at 28 days increase by 65.6% and 61.9%, respectively, which are considerably greater than those without NT. While the dosage of NT is up to 5%, the increase rates of tensile and flexural strengths at 28 days are only 35.6% and 30.3%, respectively, compared with M0. The results also indicate that the increases of tensile and flexural strengths are significant, suggesting that the toughness and crack extension resistance have apparently strengthened when the NT dosage is 3%. In general, toughness and crack extension resistance are significantly associated with tensile and flexural strengths.

The impact mechanisms of nanomaterial on flexural and tensile strengths have been proved in earlier work. When appropriate amount of nanoparticles is used in mortars, the crystal orientation of CH between hardened cement pastes and aggregates can be significantly improved and the grain size of CH is also decreased, both of which can control the crystallization process of hydration products in an appropriate state [25]. In addition, more compact C-S-H gels are formed under the nanometer hydration induction effect [26, 27], which can significantly improve the mechanical properties of cement mortars. If the dosage of nanoparticles is too high, drying shrinkage distortions of mortars are enlarged, leading to more microcracks in the interface of hardened pastes and aggregates and resulting in the reduction of flexural and tensile strengths [28, 29]. Simultaneously, excess nano-TiO_2 is difficult to spread evenly and some internal defects would likely form in mortars, which will certainly influence the tensile and flexural strengths. Beyond that, the reduction of CH content can also achieve the same effect. Based on the above analysis, it is clear that the right amount of NT (≤3%) can improve the flexural and tensile strengths of mortars remarkably, while overdosage (>3%) would be counterproductive.

Figure 4 displays the SEM images of mortars mixed with NT (0%, 3%, 4%, and 5%) at 28 days, showing that samples with different dosages of NT have obvious differences in morphology. When there is no NT, the microstructure appears as obvious acicular crystals, which are the major cement hydration products of AFt, AFm, and CH (Figure 4(a)). Increasing NT content up to 3% is linked with thick short columnar crystals, being equally distributed and interweaving to form a net (Figure 4(b)). For dosages 4% and 5%, the morphologies of hydration crystals are similar to incomplete polyhedrons (Figure 4(c)) and regular, complete, and independent polyhedrons (Figure 4(d)), respectively. These results suggest that NT is able to control the morphologies of cement hydration products. Thick short columnar crystals grow primarily in pores and soft region of mortars with 3% NT, which have a tendency to crisscross and to be interwoven from different directions, leading to the higher flexural and tensile strengths. However, the interconnections of closer packed polyhedron crystals decrease a lot, causing the reduction of flexural and tensile strengths of mortars with 5% NT.

The content of AFt forming in the hydration of mortars with different dosages of NT over time is shown in Figure 5. Results show that the amounts of AFt firstly increase and then descend with the increasing of NT and reach the peak when dosage of NT is 3% for all ages (3~90 days). For hydration at 3 days, AFt in mortars with 3% NT increases by 50.8%, which are significantly greater than that without NT. However, AFt in mortars with 4% and 5% NT is about the same as that without NT. For hydration at 28 days, the generation amounts of AFt of each sample reach the maximum compared with other ages, and the mortars with 3% NT have the highest content, which increase by 61.6% compared to the sample without NT and 28.2% compared with the same sample at 3 days. For hydration at 90 days, contents of AFt in mortars decrease by different degrees when compared to that at 28 days except the sample without NT, with the largest proportional decreases appearing at 3% NT, reducing from 17.81% to 14.56%. The reason for this is that the AFt generation is related to the concentration of sulfate ion, while the addition of inert nanoparticles can promote the early hydration of the cement [30], making mortars more compact and more sulfate ion solvated into C-S-H gel. Due to the lack of sulfate ion used to keep structures of AFt, it is easy to transform AFt into AFm. In addition, the formation of AFt is also connected to residual space of the hydration system [31]. If nanoparticles are evenly dispersed in the mortars, large specific surface areas and energy and lots of defects make the newly formed hydration products adsorbed to the surface of nanoparticles as crystal nucleus, which will accelerate the hydration of cement and accumulation

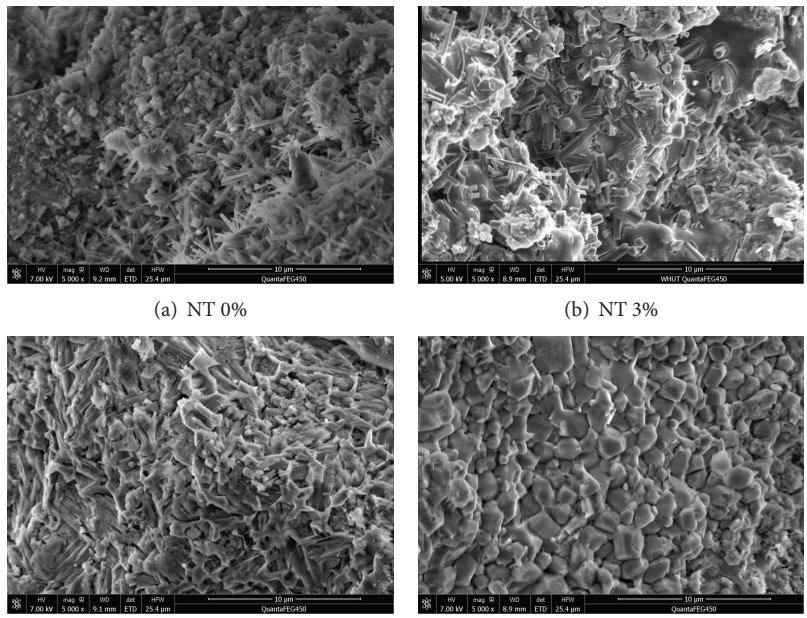

(a) NT 0% (b) NT 3%

(c) NT 4% (d) NT 5%

Figure 4: SEM images of mortars with NT at 28 days.

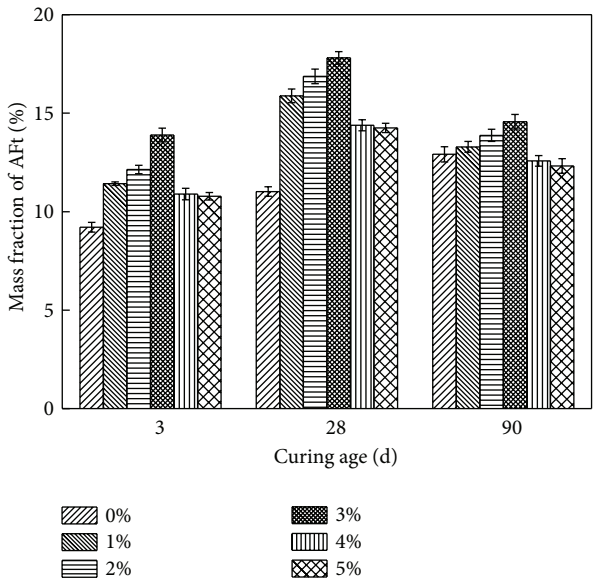

Figure 5: Contents of AFt in mortars with different dosages of NT at different ages.

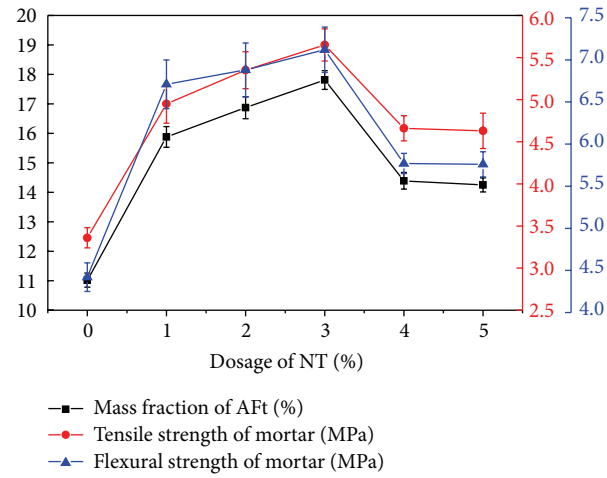

Figure 6: Relationships between flexural and tensile strengths and the AFt content at 28 days.

of hydration products. Simultaneously, uniformly distributed nanoparticles play the adhesive role that firmly bonds hydration products and transition zone together and set up a new network which takes nanoparticles as nodes on the basis of the original network structure of hardened mortars, bonding more nanoscale C-S-H gel and forming a three-dimensional network structure [32]. All of these will reduce the residual space of the mortars, which is not conducive to the growth of AFt.

The relationships between flexural and tensile strengths and the generation of AFt in mortars at 28 days are illustrated in Figure 6, where the flexural and tensile strengths correspond to the right y-axis and the mass fraction of AFt corresponds to the left y-axis. Results show that the trends of strengths over the dosage of NT are similar to that of AFt mass fraction, indicating a positive relationship between flexural and tensile strengths and AFt content.

Table 4 shows the distributions of internal pore structures of hardened mortars at 28 days, which are measured by MIP method. As can be seen from the table, total pore volume initially decreases but turns to increase after reaching a minimum with 3% NT, where total pore volume reduces by

Table 4: Internal pore distributions of hardened mortars at 28 days with different dosages of NT.

Sample	Total intruded volume/(mL/g)	Mean radius/nm	Apparent density/(g/cm^3)	Porosity/% (2 nm < d < 5 μm)	Pore size distribution/%		
					<10 nm	10–50 nm	>50 nm
M0	0.0685	13.85	2.385	15.6	3.74	10.30	1.56
M1	0.0552	9.26	2.414	12.4	4.02	6.90	1.48
M2	0.0426	7.84	2.459	11.9	4.64	5.95	1.31
M3	0.0355	6.25	2.516	10.2	5.15	4.03	1.02
M4	0.0573	9.56	2.402	13.1	3.98	7.61	1.51
M5	0.0569	9.35	2.410	13.3	3.95	7.80	1.55

Table 5: Water absorption coefficient of hardened mortars and concretes at 28 days.

Samples	Water-to-cement ratio	Curing regime after surface treatment	Control	3% NT + unsealed	3% NT + sealed
			Water absorption coefficient/standard deviation		
Mortar	0.58	50°C/95% RH/14 days	(0.328 ± 0.010)/100%	(0.156 ± 0.012)/52%	(0.096 ± 0.016)/71%
		20°C/95% RH/14 days	(0.372 ± 0.018)/100%	(0.205 ± 0.012)/45%	(0.118 ± 0.011)/68%
Concrete	0.45	20°C/95% RH/14 days	(0.442 ± 0.014)/100%	(0.249 ± 0.011)/44%	(0.302 ± 0.015)/32%
	0.58		(0.640 ± 0.018)/100%	(0.351 ± 0.014)/45%	(0.291 ± 0.012)/55%

48.2%, harmless pores (d < 10 nm) increase by 37.7%, and harmful pores ($d \geq 50$ nm) reduce by 34.6% compared with the blank sample, indicating that the pores of mortars mixed with 3% NT are significantly refined and shift to harmless pores. When the content of NT is more than 3%, the total pore volume and the amount of harmful pores begin to increase. This could be due to the fact that the crystallization process of hydration products could be controlled in an appropriate state by restraining the growth of CH crystal when the dosage of nanomaterials and the distance between particles are moderate [25]. And also, high surface activity of nanoparticles as nucleuses in mortars can further improve the hydration reaction rate. Therefore, the hydration products accumulated quickly and then filled the water holes, leading to the reduction of porosity. What is more, the filling effect of nanomaterials can also reduce the pore volume [29]. Hence, appropriate dosage of NT can make mortars more uniform and compact. However, when the addition of NT is excessive, huge specific surface area of nanoparticles will absorb more water and make the agglomeration phenomena easily accessible, leading to the formation of undisrupted pockets within the paste matrix and resulting in an increase in porosity of mortars [30]. And Table 4 also shows that the change rules of mean radius and porosity are similar to that of total pore volume and when the amounts of pores go down, the apparent densities of hardened mortars increase; that is to say, pore structures are improved.

3.2. Influence of NT on Durability of Mortars/Concretes. Water absorption and gas erosion resistance are important technical indexes used to measure the durability of cement-based materials. In order to investigate the influence of NT on durability of mortars and concretes, water absorption and gas erosion resistance of mortars and concretes without and with 3% NT were studied.

3.2.1. Influence of NT on Water Absorption of Mortars/Concretes. The water absorption of cement-based materials relates to their own porosity and it is higher when the porosity is larger. Figure 7 and Table 5 show the results of water absorption ratio and its coefficient of the control sample and hardened mortars/concretes with 3% NT, respectively. It is evident from Figure 7 that the water absorption ratio of mortars/concretes with 3% NT decreases significantly. For unsealed mortars, water absorption ratio at 1.5 h reduces by approximately 40%, while that of sealed could reduce by around 50–60% compared with the control sample. And from the experimental data of 20°C and 50°C, it is obvious that increasing of curing temperature could not markedly improve the compactness of mortars, as shown in Figures 7(a) and 7(b). For concretes with w/c (water and cement ratio) of 0.45 and 0.58, compared with the control sample, the reduction of water absorption ratio of concretes with 3% NT is about 45–65% at 1.5 h and becomes more apparent with the increasing of w/c, as shown in Figures 7(c) and 7(d).

Table 5 shows the water absorption coefficients after processing data from Figure 7. Note that all the water absorption coefficients of mortars/concretes with 3% NT fall by more than 40% compared with the control sample.

3.2.2. Influence of NT on Gas Erosion Resistance of Mortars. The gas erosion resistance of mortars can be reflected by water-vapour permeability coefficient. Before the wet cup test, the samples should be placed for 14 days under natural conditions (relative humidity of 60%), making the humidity of samples balance inside and outside.

Figure 8 shows the curve of mass variation of wet cup over time when mortars (w/c = 0.58, 28-day hydration) are used to do the permeability test. The water-vapour permeability coefficient can be calculated by linear regression and the area of the sample after the mass change of wet cup is steady. The calculation results show that the water-vapour permeability coefficients of control sample and mortars with 3% NT are 3.12×10^{-6} g·h^{-1}·mm^{-2} and 1.75×10^{-6} g·h^{-1}·mm^{-2}, respectively, indicating that modification with NT can decrease the permeability coefficients of mortars by 43.9%. From the above

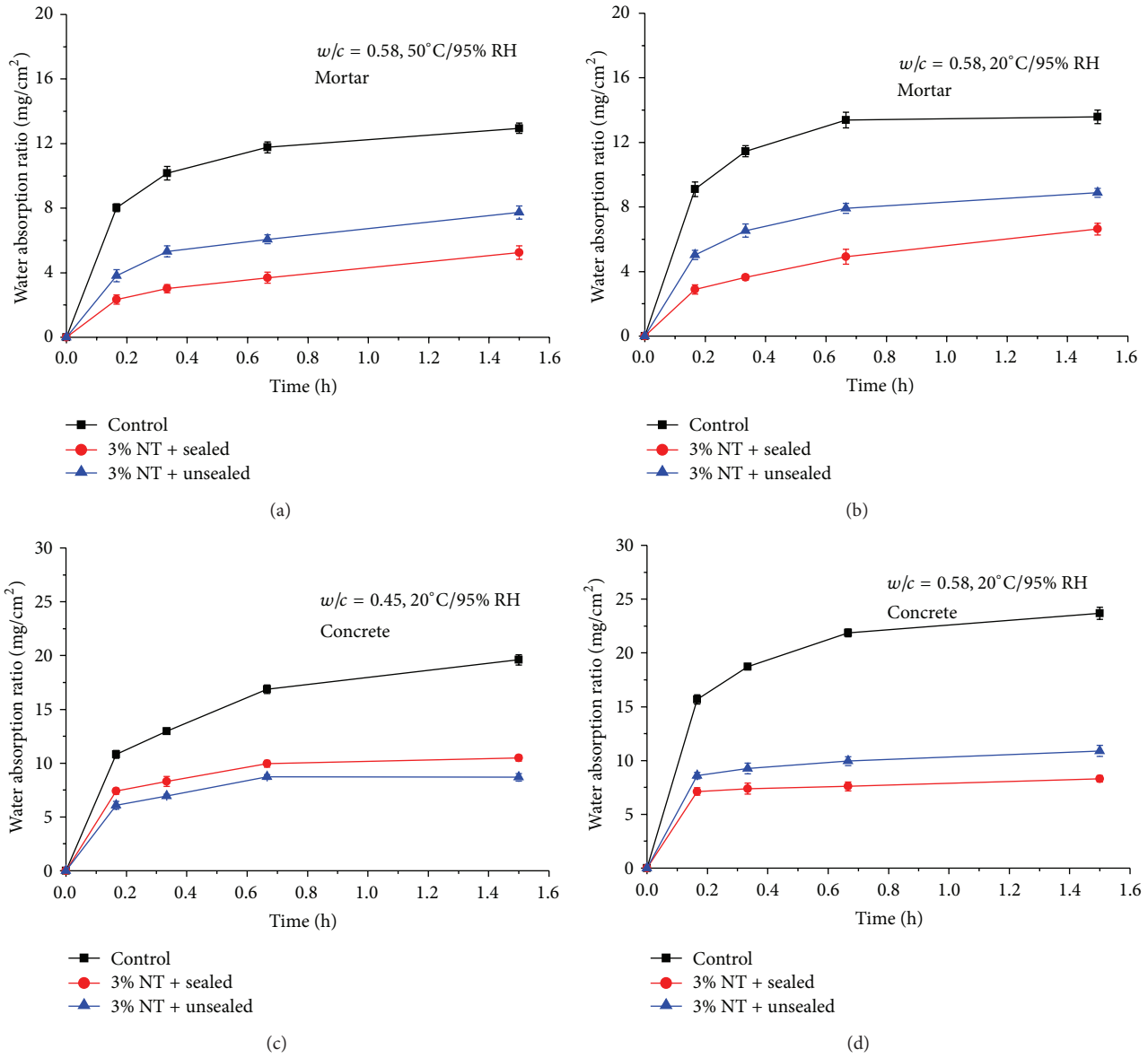

Figure 7: Influence of NT on the water absorption of hardened mortars and concretes at 28 days.

analysis, a conclusion can be drawn that the addition of 3% NT can significantly improve the gas erosion resistance of mortars.

3.3. Regulation Mechanism of NT on Cement Hydration Products. In the hydration process, the cement clinker particles will carry out a complex hydration reaction to form ettringite (AFt), AFm, calcium hydroxide (CH), and calcium silicate hydrate (C-S-H) gel. Generally, CH, Aft, and AFm exhibit rod-like and needle-like shapes with disorder, which determines the brittleness of cement samples [32]. According to the results and discussion above, the hydration models of cement mixtures with 0% and 3% NT at 28 days can be proposed as shown in Figure 9.

Figure 9 depicts the formation of hydration products at 28 days, where these hydration products are shown to form on the unhydrated cement particle surface as well as on the NT surface. However, the morphology and size of hydration products of these two systems are relatively different. After being mixed with NT, AFt crystals are easier to form on the surface of unhydrated cement and NT particles, where AFt changes from slender needles to short rods and then intersects to form a complex network. Such phenomenon shows that the growth points and growth pattern of the hydration products are both controlled by NT, which is called a nuclei effect. Therefore, NT can provide nucleation sites, which accelerate the precipitation of hydration products, make C-S-H disperse better, and limit the growth of CH, thus improving the density and homogeneity of cement matrix [15]. Simultaneously, the physical effects of NT, including filling and interlocking, can reduce the porosities and bridge failure planes of cement matrix, thus improving the microstructure of matrix. As shown in Figure 9, incorporating NT also makes the pore structures thinner. All of these microstructure

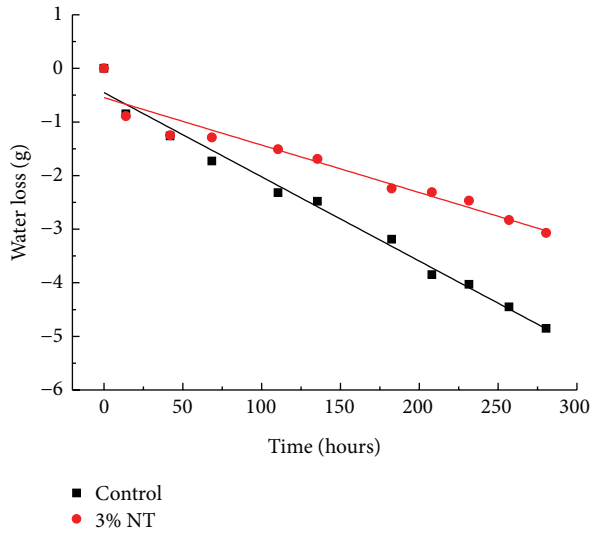

Figure 8: Water-vapour permeability of mortars before and after NT-modification ($w/c = 0.58$).

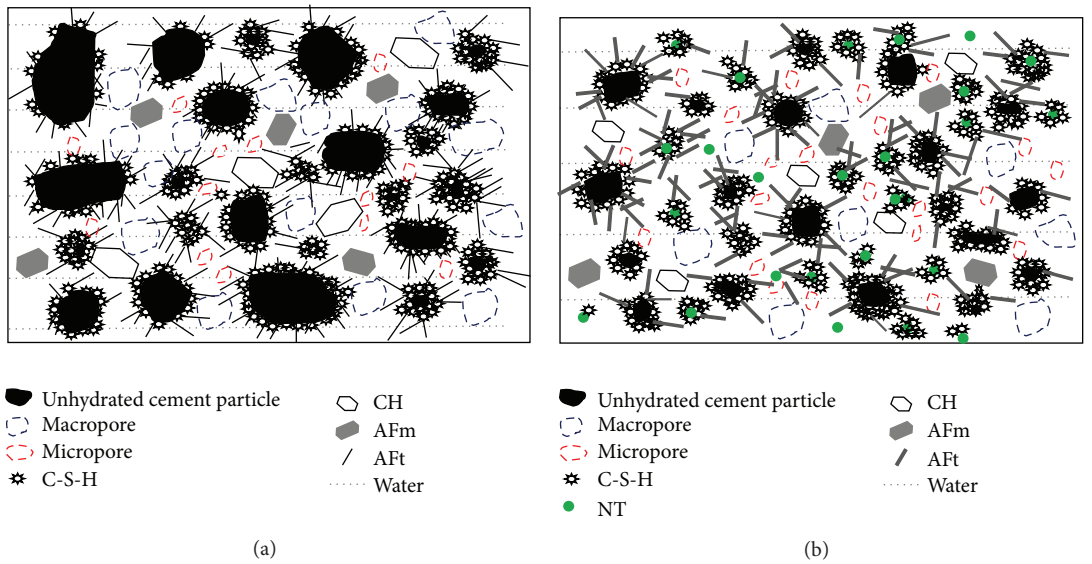

Figure 9: Hydration models of cement mixtures with (a) 0% NT and (b) 3% NT addition at 28 days.

changes have greatly contributed to improving toughness and durability of cement composites.

4. Conclusion

(1) At 28 days, the mortars with 3% NT exhibit significant increase in tensile strength (65.6%), flexural strength (61.9%), the content of AFt (61.6%), and the harmless pores (37.7%) compared to those without NT. Accordingly, the total pore volume and the harmful pores reduce by 48.2% and 34.6%, respectively. The results indicate that the addition of NT can significantly refine the pores and make them shift to harmless pores.

(2) When the dosage of NT is more than 3% at 28 days, the morphologies of hydration products (AFt) are changed from short columnar (3% NT, at 28 days) into mainly complete or incomplete polyhedral, and the flexural and tensile strengths and the amounts of AFt are decreased simultaneously compared to those with 3% NT. The results show that NT plays an important role in regulating the microstructure of hydration products and there is a positive relationship between flexural and tensile strengths and AFt content.

(3) When the content of NT is 3% at 28 days, the water absorption ratio decreases by 40–65%, the water absorption coefficient falls by more than 40%, and the water-vapour permeability coefficient of mortars decreases by 43.9% compared to those without NT.

(4) The main causes of improving the toughness and the compactness of cement-based materials are

nucleation effect, improving crystallization orientation of CH and controlling grain size effect, and microaggregate filling effect of NT in the cement hydration process.

In summary, 3% NT can significantly improve the toughness, structure compactness, and durability and effectively avoid the high brittleness of cement-based materials.

Conflict of Interests

The authors declare that there is no conflict of interests regarding the publication of this paper.

Acknowledgments

This work was supported by the National Natural Science Foundation of China (no. 51378408) and the Fundamental Research Funds for the Central Universities (no. 2013-YB-25).

References

[1] K. Hashimoto, H. Irie, and A. Fujishima, "TiO_2 photocatalysis: a historical overview and future prospects," *Japanese Journal of Applied Physics*, vol. 44, no. 12, pp. 8269–8285, 2005.

[2] A. Fujishima and X. Zhang, "Titanium dioxide photocatalysis: present situation and future approaches," *Comptes Rendus Chimie*, vol. 9, no. 5-6, pp. 750–760, 2006.

[3] H. Ichiura, T. Kitaoka, and H. Tanaka, "Removal of indoor pollutants under UV irradiation by a composite TiO_2-zeolite sheet prepared using a papermaking technique," *Chemosphere*, vol. 50, no. 1, pp. 79–83, 2003.

[4] J. Chen and C.-S. Poon, "Photocatalytic activity of titanium dioxide modified concrete materials—influence of utilizing recycled glass cullets as aggregates," *Journal of Environmental Management*, vol. 90, no. 11, pp. 3436–3442, 2009.

[5] M. Chen and J.-W. Chu, "NO_x photocatalytic degradation on active concrete road surface—from experiment to real-scale application," *Journal of Cleaner Production*, vol. 19, no. 11, pp. 1266–1272, 2011.

[6] J. G. Yu, J. X. Low, W. Xiao, P. Zhou, and M. Jaroniec, "Enhanced photocatalytic CO_2-reduction activity of anatase TiO_2 by Co-exposed {001} and {101} facets," *Journal of the American Chemical Society*, vol. 136, no. 25, pp. 8839–8842, 2014.

[7] D. Osborn, M. Hassan, and H. Dylla, "Quantification of reduction of nitrogen oxides by nitrate accumulation on titanium dioxide photocatalytic concrete pavement," *Transportation Research Record*, no. 2290, pp. 147–153, 2012.

[8] N. Bengtsson and M. Castellote, "Heterogeneous photocatalysis on construction materials: effect of catalyst properties on the efficiency for degrading NO_x and self cleaning," *Materiales de Construccion*, vol. 64, no. 314, article e013, 2014.

[9] M. V. Diamanti, B. Del Curto, M. Ormellese, and M. P. Pedeferri, "Photocatalytic and self-cleaning activity of colored mortars containing TiO_2," *Construction and Building Materials*, vol. 46, pp. 167–174, 2013.

[10] A. Folli, C. Pade, T. B. Hansen, T. De Marco, and D. E. MacPhee, "TiO_2 photocatalysis in cementitious systems: insights into self-cleaning and depollution chemistry," *Cement and Concrete Research*, vol. 42, no. 3, pp. 539–548, 2012.

[11] T. Maggos, A. Plassais, J. G. Bartzis, C. Vasilakos, N. Moussiopoulos, and L. Bonafous, "Photocatalytic degradation of NO_x in a pilot street canyon configuration using TiO_2-mortar panels," *Environmental Monitoring and Assessment*, vol. 136, no. 1–3, pp. 35–44, 2008.

[12] T. Yuranova, V. Sarria, W. Jardim et al., "Photocatalytic discoloration of organic compounds on outdoor building cement panels modified by photoactive coatings," *Journal of Photochemistry and Photobiology A: Chemistry*, vol. 188, no. 2-3, pp. 334–341, 2007.

[13] C. A. Linkous, G. J. Carter, D. B. Locuson, A. J. Ouellette, D. K. Slattery, and L. A. Smitha, "Photocatalytic inhibition of algae growth using TiO_2, WO_3, and cocatalyst modifications," *Environmental Science & Technology*, vol. 34, no. 22, pp. 4754–4758, 2000.

[14] K. Demeestere, J. Dewulf, B. de Witte, A. Beeldens, and H. van Langenhove, "Heterogeneous photocatalytic removal of toluene from air on building materials enriched with TiO_2," *Building and Environment*, vol. 43, no. 4, pp. 406–414, 2008.

[15] B. Y. Lee and K. E. Kurtis, "Influence of TiO_2 nanoparticles on early C_3S hydration," *Journal of the American Ceramic Society*, vol. 93, no. 10, pp. 3399–3405, 2010.

[16] K. Watanabe, T. Kimura, and J. Niwa, "Synergetic effect of steel fibers and shear-reinforcing bars on the shear-resistance mechanisms of RC linear members," *Construction and Building Materials*, vol. 24, no. 12, pp. 2369–2375, 2010.

[17] M. Z. Hossain and A. S. M. A. Awal, "Flexural response of hybrid carbon fiber thin cement composites," *Construction and Building Materials*, vol. 25, no. 2, pp. 670–677, 2011.

[18] M. Ali, A. Liu, H. Sou, and N. Chouw, "Mechanical and dynamic properties of coconut fibre reinforced concrete," *Construction and Building Materials*, vol. 30, pp. 814–825, 2012.

[19] J. M. L. Reis, "Fracture and flexural characterization of natural fiber-reinforced polymer concrete," *Construction and Building Materials*, vol. 20, no. 9, pp. 673–678, 2006.

[20] P. Soroushian, J.-P. Won, and M. Hassan, "Durability characteristics of CO_2-cured cellulose fiber reinforced cement composites," *Construction and Building Materials*, vol. 34, pp. 44–53, 2012.

[21] H. Y. Su and J. Y. Xu, "Dynamic compressive behavior of ceramic fiber reinforced concrete under impact load," *Construction and Building Materials*, vol. 45, pp. 306–313, 2013.

[22] N. Morova, "Investigation of usability of basalt fibers in hot mix asphalt concrete," *Construction and Building Materials*, vol. 47, pp. 175–180, 2013.

[23] J. M. Khatib and P. S. Mangat, "Absorption characteristics of concrete as a function of location relative to casting position," *Cement and Concrete Research*, vol. 25, no. 5, pp. 999–1010, 1995.

[24] ASTM International, *ASTM E96-00, Standard Test Methods for Water Vapor Transmission of Materials*, ASTM International, West Conshohocken, Pa, USA, 2000.

[25] T. Ji, "Preliminary study on the water permeability and microstructure of concrete incorporating nano-SiO_2," *Cement and Concrete Research*, vol. 35, no. 10, pp. 1943–1947, 2005.

[26] B. Y. Lee, A. R. Jayapalan, and K. E. Kurtis, "Effects of nano-TiO_2 on properties of cement-based materials," *Magazine of Concrete Research*, vol. 65, no. 21, pp. 1293–1302, 2013.

[27] A. R. Jayapalan, B. Y. Lee, S. M. Fredrich, and K. E. Kurtis, "Influence of additions of anatase TiO_2 nanoparticles on early-age properties of cement-based materials," *Transportation Research Record*, no. 2141, pp. 41–46, 2010.

[28] H. W. Song, K. J. Byun, S. H. Kim, and D. H. Choi, "Early-age creep and shrinkage in self-compacting concrete incorporating GGBFS," in *Proceedings of the 2nd International RILEM Symposium on Self-Compacting Concrete*, pp. 413–422, Tokyo, Japan, 2001.

[29] P. Turcry and A. Loukili, "A study of plastic shrinkage of self-compacting concrete," in *Proceedings of the 3rd International RILEM Symposium on Self-Compacting Concrete*, pp. 576–585, Reykjavik, Iceland, 2003.

[30] J. Chen, S.-C. Kou, and C.-S. Poon, "Hydration and properties of nano-TiO_2 blended cement composites," *Cement and Concrete Composites*, vol. 34, no. 5, pp. 642–649, 2012.

[31] R. S. Gollop and H. F. W. Taylor, "Microstructural and micro-analytical studies of sulfate attack. II. Sulfate-resisting Portland cement: ferrite composition and hydration chemistry," *Cement and Concrete Research*, vol. 24, no. 7, pp. 1347–1358, 1994.

[32] H. Li, H.-G. Xiao, J. Yuan, and J. P. Ou, "Microstructure of cement mortar with nano-particles," *Composites, Part B: Engineering*, vol. 35, no. 2, pp. 185–189, 2004.